Available online at www.sciencedirect.com

SciVerse ScienceDirect

Geochimica et Cosmochimica Acta 75 (2011) 7446–7457

Geochimica et Cosmochimica Acta

www.elsevier.com/locate/gca

Phosphate defects and apatite inclusions in coral skeletal aragonite revealed by solid-state NMR spectroscopy

Harris E. Mason [a,*,1], Paolo Montagna [b,c,2], Laura Kubista [a], Marco Taviani [b,d], Malcolm McCulloch [e], Brian L. Phillips [a]

[a] Department of Geosciences, Stony Brook University, Stony Brook, NY 11794-2100, USA
[b] Istituto di Scienze Marine (ISMAR), Consiglio Nazionale delle Ricerche (CNR), Via P. Gobetti 101, 40122 Bologna, Italy
[c] Lamont-Doherty Earth Observatory Columbia University, 61 Route 9W, Palisades, NY 10964, USA
[d] Woods Hole Oceanographic Institution, 266 Woods Hole Road, MA 02543, USA
[e] School of Earth and Environment, The University of Western Australia (M004), 35 Stirling Highway, Crawley WA 6009, Australia

Received 15 March 2010; accepted in revised form 3 October 2011

Abstract

Recent development of paleo-nutrient proxies based on the phosphorus/calcium (P/Ca) ratio in tropical- and deep-water corals (also known as cold-water corals) require an understanding of the processes by which P is incorporated into the coral skeletal aragonite. Here, we apply single- and double-resonance solid-state nuclear magnetic resonance (NMR) spectroscopy to determine the speciation of P in coral aragonite. The results show that the majority of P occurs as phosphate defects in the aragonite structure, but in many samples a significant fraction of the P occurs also in crystalline hydroxylapatite inclusions. Quantification of the amount of hydroxylapatite indicates that its presence is not related simply to external environmental factors and that it can occur at varying abundances in different parts of the same corallite. Since there is currently no model available to describe the relationship between dissolved inorganic phosphate and its incorporation as apatite inclusions into carbonates, careful screening of samples which contain only phosphate in the aragonite structure or selective microsampling could improve proxy development.
Published by Elsevier Ltd.

1. INTRODUCTION

It has been recently proposed that P/Ca ratios in the aragonite skeleton of corals record the ambient concentration of dissolved inorganic phosphorus (DIP), which, when combined with U-series chronology, could prove to be a useful paleo-nutrient proxy (Montagna et al., 2006; Anagnostou et al., 2007, 2011; LaVigne et al., 2008, 2010). The amount of bioavailable phosphate in the photic zone of the surface ocean limits primary productivity in some ocean basins (Tyrrell, 1999; Benitez-Nelson, 2000). Since export of biomass to deep waters may act to drawdown atmospheric CO_2 (Broecker, 1982; Volk and Hoffert, 1985; Sarmiento et al., 1998), knowledge of past oceanic P concentrations is important to estimate the contribution of the "biological pump" to regulate the levels of atmospheric CO_2. Montagna et al. (2006) noted that laser ablation inductively coupled plasma mass spectrometry (LA-ICPMS)-derived P/Ca ratios for aragonite septa from a variety of recent *Desmophyllum dianthus* coral samples were linearly related to the DIP concentration of the waters from which they were collected. This correlation was used to reconstruct paleo-nutrient data from a ~11,190 year old sample. Unlike other trace elements used as paleo-environmental proxies such as Ba, Sr, and Cd, P cannot substitute simply into the aragonite crystal structure

* Corresponding author. Address: 7000 East Ave. L-231, Livermore, CA 94551-0808, USA. Tel.: +1 925 423 1041.
E-mail address: mason42@llnl.gov (H.E. Mason).
[1] Present address: Physical Life Sciences Directorate, Lawrence Livermore National Laboratory, Livermore, CA 94550, USA.
[2] Present address: Laboratoire des Sciences du Climat et l'Environnement, Gif-sur-Yvette 91198, France.

0016-7037/$ - see front matter Published by Elsevier Ltd.
doi:10.1016/j.gca.2011.10.002

and its form in the coral aragonite is unknown (Dodge et al., 1984). Furthermore, the P speciation can be reasonably expected to influence the relationship between DIP concentration and aragonite P/Ca.

Geochemical models of trace element incorporation in calcite and aragonite typically rely on thermodynamic treatment of incorporation of the trace element into the mineral structure (Cohen and McConnaughey, 2003; Gaetani and Cohen, 2006; Gagnon et al., 2007). Phosphate co-precipitation, sorption, and desorption studies at phosphate solution concentrations less than 100 μM and near neutral pH suggest that inorganic phosphate incorporation in calcite can be modeled by adsorption and subsequent incorporation of protonated phosphate groups (House and Donaldson, 1986; Hinedi et al., 1992; Millero et al., 2001). It has also been shown, in certain cases, that calcite with 60–100 μg P/g can contain crystalline Ca-phosphate inclusions that are difficult to detect by microanalytical methods, suggesting that surface precipitates can form and be subsequently encapsulated by continued crystal growth (Mason et al., 2007). Crystalline Ca-phosphates can be difficult to nucleate and models that could account for the formation of such P-rich precipitates via heterogeneous nucleation on calcium carbonate surfaces (Koutsoukos and Nancollas, 1981) have yet to be fully explored. Therefore, to model the co-precipitation of phosphate with calcium carbonate minerals it is desirable that phosphate be incorporated as a structural constituent.

Solid-state ^{31}P nuclear magnetic resonance (NMR) spectroscopy is one potential technique from which information on the distribution of P in coral aragonite might be obtained. The ^{31}P NMR chemical shift is very sensitive to the bonding environment surrounding P and has distinct, often characteristic, values for crystalline phases. ^{31}P NMR techniques, primarily in the solution phase, have been used extensively to determine P-speciation in soluble extracts of soil samples, marine sediments, and particulate matter (for a review of these ^{31}P studies see Cade-Menun (2005) and Turner et al. (2005) for a review of extraction methods). These methods are highly sensitive to organic P-species and are required for NMR investigation of materials containing significant concentrations of paramagnetic ions (which cause severe line broadening in NMR spectra), but require harsh chemical treatments to separate various P fractions. In addition, only a fraction of the P is typically extracted from the solids (30–60% recovery), with some P remaining in the insoluble residue (Ahlgren et al., 2007). Considering that coral aragonite typically contains low concentrations of Fe and Mn, and bulk P concentrations just within the NMR detection limit, it might be amenable to investigation by *in situ* solid-state ^{31}P NMR methods.

Here, we present a survey of solid-state ^{31}P NMR spectra of coral skeletal material that illustrates the potential of the technique for determining the speciation of P in such materials as well as in other carbonate minerals. We use a variety of solid-state NMR spectroscopic methods to characterize inorganic phosphate in a synthetic aragonite/phosphate coprecipitate and show that the phosphate occurs within a few Å of several carbonate groups, indicating that it is incorporated in the aragonite structure. The similarity of these data with those obtained for coral skeletal material provides strong evidence that structural phosphate defects are the principal P-species in coral aragonite. Many coral samples also yield a ^{31}P NMR signal characteristic of crystalline apatite that can account for a significant fraction of the bulk P, but its origin is uncertain. These results support the use of P/Ca ratios for paleoenvironmental proxies, but also suggest that the proxy relationships might be improved by selecting samples lacking apatite inclusions.

2. EXPERIMENTAL METHODS

2.1. Sample preparation

2.1.1. Coral Samples

Subsamples of coral skeleton were selected from modern and subfossil corals lacking any visible Fe–Mn-rich crust, upon observation under a binocular microscope and using thin sections in plane and cross-polarized light. No major visible alterations (e.g. diagenetic alteration or bioerosions) were evident. The P/Ca ratios and the P concentration of the coral samples were obtained using LA-ICPMS following the procedures described by Montagna et al. (2006) and through solution ICPMS analysis (see method below).

The sampling methods differed among the various coral species.

D. dianthus and *Flabellum* sp.: fragments of the largest septum S1 were carefully removed with a diamond tipped saw attached to a dentist drill. Other sub-samples were cut from the thecal wall and all the fragments of septa attached to the theca were mechanically abraded away using the same dentist drill. This allowed us to obtain samples representative of both the septum and the thecal margin. Two sub-samples of *D. dianthus* septa were crushed to pass a 250 μm analytical sieve and subjected to chemical cleaning; one was placed in a bleach solution (6% NaClO) and agitated for 4 days. The second sub-sample was ultrasonically washed for 10 min in deionized water, 3 min in a 0.15 N HNO_3 solution, 20 min in a 1:1 oxidizing mixture of 30% H_2O_2 and 0.2 N HNO_3 with alternated heating in a boiling water bath, and a final 3 min in 0.15 N HNO_3. Both cleaned sub-samples were then rinsed with deionized water and dried in a 60 °C oven overnight. The latter method is similar to those prescribed by Shen and Boyle (1988), Cheng et al. (2000), and LaVigne et al. (2008) which are designed to remove sorbed metals and metal oxide coatings.

Lophelia pertusa: pieces of the thecal wall were obtained by cutting single corallites transversally. The part corresponding to the intersection between the wall and the septa (inside edge of the theca) was abraded and septa were completely removed.

Madrepora oculata: a piece of the coral was collected by cutting a corallite transversally. This coral portion con-

tains both the thecal wall and the septa ("whole coral" reported in the text).

Porites sp.: a small rectangular parallelepiped was removed from a 7 mm slab previously obtained by cutting a coral core along the axis of growth. The subsample was taken 12 cm from the top of the coral core in order to avoid remnants of coral tissue.

2.1.2. Synthetic aragonite/phosphate coprecipitates

Aragonite/phosphate co-precipitation was undertaken using a seeded constant addition method adapted from Zhong and Mucci (1993) and described by Reeder et al. (2000). The aragonite seeds were synthesized by pumping separate solutions of 0.2 M $CaCl_2$ and 0.2 M Na_2CO_3 using a dual syringe pump at a rate of 300 μl/min into an initial solution containing 7 mM $CaCl_2$, 7 mM $NaHCO_3$, and 50 mM $MgCl_2$ through which air was being bubbled and which was stirred with a suspended PTFE stir bar. Each solution contained 0.1 M NaCl as background electrolyte. The reaction was allowed to proceed for 4.5–5 h, after which the solids were collected by vacuum filtration through a 0.2 μm membrane filter, rinsed several times with deionized water to remove residual salts, and dried in a 60 °C oven overnight. The dried aragonite seeds were stored in a sealed borosilicate glass container prior to their use in further experiments. The aragonite seeds were identified as pure aragonite by powder X-ray diffraction and analyzed by scanning electron microscopy (SEM) to determine the average dimensions and morphology of the crystals, revealing blocky crystals typically 3 μm wide by 4–10 μm long grouped into ball-shaped clusters 40–50 μm in diameter. For the phosphate co-precipitation experiments, the same procedure was used except that 0.1 g of aragonite seed material was added to the initial growth solution to provide nucleation sites, the concentrations of reactants in the syringes were 0.1 M, and $NaHPO_4$ was added to the carbonate syringe such that the phosphate concentration of the syringe ranged from 50 to 100 μM. Periodically, aliquots of the growth solution were drawn from the reactor to analyze total carbonate and reactive phosphate concentrations, from which we determined that the phosphate concentration ranged from 1 to 3 μM during crystal growth. The P concentration of the overgrowths was calculated from the difference between the amount phosphate added to the solution and what remained in solution at the end of the experiment (from the measured reactive phosphate concentration and total solution volume), whereas the mass of calcium carbonate precipitated was estimated from the difference between the amount of Ca added to the growth solution and what remained in solution at the end of the experiment (estimated from the final total carbonate concentration). A ^{13}C-enriched aragonite/phosphate coprecipitate was prepared similarly by substitution of a 0.1 M $NaH^{13}CO_3$ solution in the Na_2CO_3 syringe. This sample was used only for the $^{31}P/^{13}C$ double resonance NMR experiments, for which the natural abundance of the NMR-active ^{13}C isotope (1.1%) is too low to observe spectroscopic effects. Powder X-ray diffraction indicates that most of the synthetic coprecipitates contained only aragonite. Some of the samples contained calcite (up to 9%; Milliman and Bornhold, 1973; Morse et al., 1985), but these were not used for NMR analysis.

2.2. Laser ablation ICPMS analysis

The P/Ca ratios and the P concentrations were obtained following the analytical method by Montagna et al. (2006, 2007). We used a high sensitivity pulsed laser ablation system, coupled with a Fison PQII ICPMS with enhanced sensitivity. This laser ablation system, housed at RSES (Canberra), uses a LambdaPhysik LPX 120i argon fluoride 193 nm excimer laser. All the coral samples were scanned at 20 μm/s using a 20 μm wide and 220 μm long rectangular laser beam mask with the laser pulsing at 5 Hz and an energy of 50 MJ. Before acquisition, surface contamination was removed by pre-ablating the coral surfaces twice with a 230 μm diameter spot followed by the same rectangular slit used for the analysis. A pressed powder coral disc and the NIST glass standard 612, chosen because its P concentration is comparable to the coral samples, were analyzed before and after each run on the samples, together with the acquisition of the background (gas blank) for 60 s, allowing correction for long-term instrumental drift during analysis. The precision for ^{31}P, calculated as the RSD (1σ/mean) of 60 s acquisition on the NIST 612 was ~6%.

The P concentrations of *D. dianthus* and *Flabellum* sp. were obtained both on the outer faces of the S1 septum and on the thecal wall, whereas *L. pertusa* was only analyzed along the theca. In the case of the *Porites* coral, it was not possible to discriminate between the theca and the septa and, thus, the P concentration represents an average over these skeletal components.

2.3. Bulk solution ICPMS analysis

Analyses of ^{31}P and ^{43}Ca on solutions of acid-digested coral aragonite were determined by inductively coupled plasma mass spectrometry (ICP-MS) using the multi-collector Axiom in single collection mode at Lamont-Doherty Earth Observatory and following the standard addition method (Vandecasteele and Block, 1997) to correct for the matrix effect.

For some of the samples analyzed by ^{31}P NMR, a precisely-weighted amount of coral powder was dissolved in double distilled HNO_3 and further diluted in 1% HNO_3 for the analysis by ICPMS. Procedural blank solutions were made with the same vials and acid used for the treatment of the samples. The analyses were carried out in two separate sessions. In the first session, the concentration of P was measured in solutions at a final dilution factor of ~2000:1. For the second session, the solutions were further diluted to a dilution factor of ~6000:1 and analyzed for calcium.

A multi-element stock standard mixture was prepared gravimetrically in 1% HNO_3 using High-Purity Standards (Charleston, SC; 1000 ± 3 μg/ml in 0.05% HNO_3 v/v for P; 1000 ± 3 μg/ml in 3% HNO_3 v/v for Mg and Sr; 10

μg/ml in 4% HNO_3 for Ca), mixed in appropriate concentrations to match the typical composition of coral skeletons. Two four-point standard curves were constructed by adding increasing volumes of the stock solution to six pre-cleaned vials containing a fixed volume of the unknown solutions (sample "G15606 S" and "DD Chile S-ct") and 1% HNO_3. The first point of each standard curve consists of the unspiked original sample. A third three-point standard curve was obtained by adding increasing amounts of a stock solution containing solely P (High-Purity Standards) to pre-cleaned vials having a fixed volume of the unknown solution (sample "G16505 S") and 1% HNO_3. The results of the two standardization methods were compared to verify the quality of the measurements.

A drift correction was performed by analyzing an indium spiked mixed solution after every five samples and using a linear interpolation for all the elements. All the working solutions were also spiked with indium as an internal standard to further correct for the instrumental drift. The standards and unknown solutions were introduced to the plasma by a self-aspirating nebulizer with an uptake rate of ~30 μl/min in conjunction with a Cetac Aridus desolvating system. Analytical reproducibility based on the RSD (1σ/mean) of 10 analyses of the Porites coral standard JCp-1 (Geological Survey of Japan; run as an unknown) was $\sim \pm 9.5\%$ for P/Ca and P concentration. Procedural blank for P, which was subtracted from the sample raw counts, was typically <20% of the sample signal.

2.4. Solid-state NMR spectroscopy

The ^{31}P single pulse magic angle spinning (SP/MAS) NMR and $^{31}P\{^{1}H\}$ cross polarization (CP) MAS NMR spectra were collected on a 400 MHz Varian Inova spectrometer at operating frequencies of 161.8 and 399.8 MHz for ^{31}P and ^{1}H, respectively. Samples were contained in 7.5 mm outside diameter (o.d.) Si_3N_4 rotors and spun at 5 kHz. The probe and rotor assemblies yielded no detectable ^{31}P NMR signal after several days of acquisition, but standard ZrO_2-based rotor sleeves can give a broad, weak ^{31}P signal in the orthophosphate region (here taken to be the ^{31}P spectral region from −5 to 12 ppm; Turner et al., 1986). The ^{1}H SP/MAS NMR and $^{1}H\{^{31}P\}$ rotational echo double resonance (REDOR) spectra were obtained using a Chemagnetics probe assembly configured for 4 mm (o.d.) rotors and modified to yield a very low ^{1}H background signal. The ^{1}H background signal is approximately 30 times less intense than that from the sample and was not subtracted from the spectra. The $^{31}P\{^{1}H\}$ Heteronuclear Correlation (HetCor) spectra were obtained using a probe configured for 3.2 mm (o.d.) rotors and were collected as a total of 100 hypercomplex points in *t1* with a 10 μs increment, corresponding to a 100 kHz spectral window in the ^{1}H dimension. A Carr–Purcell–Meiboom–Gill (CPMG) type acquisition was implemented to shorten the time needed to perform the HetCor experiment. The $^{19}F\{^{31}P\}$ REDOR, $^{31}P\{^{13}C\}$ SP/REDOR, and $^{1}H \rightarrow {}^{31}P\{^{13}C\}$ CP/REDOR spectra were collected on a 500 MHz Varian Infinity Plus spectrometer at operating frequencies of 125.7, 202.3, 470.2, and 499.8 MHz for ^{13}C, ^{31}P, ^{19}F and ^{1}H respectively. The $^{19}F\{^{31}P\}$ REDOR spectra were collected using a Varian/Chemagnetics T3-type probe configured for 3.2 mm (o.d.) rotors and to give a very low ^{19}F background. Empty rotor assemblies yielded no detectable ^{19}F NMR signal after 2 days of acquisition under similar conditions. The $^{31}P\{^{13}C\}$ SP and $^{1}H \rightarrow {}^{31}P\{^{13}C\}$ CP/REDOR spectra were collected using a Varian HXY probe configured for 4 mm (o.d) rotors. The ^{31}P MAS NMR spectra are referenced with respect to 85% phosphoric acid using hydroxylapatite as a secondary reference set to 2.65 ppm. The ^{1}H MAS NMR spectra are referenced with respect to tetramethylsilane using hydroxylapatite as a secondary reference set to 0.2 ppm. The ^{19}F spectra were referenced with respect to CCl_3F ($C_6F_6 = 142$ ppm).

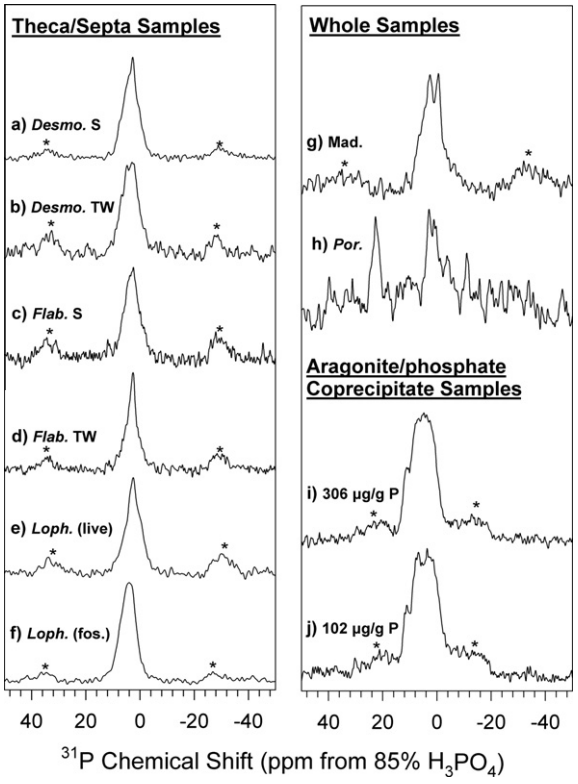

Fig. 1. ^{31}P NMR spectra for coral aragonite and aragonite/phosphate coprecipitate samples. (a–f) $^{31}P\{^{1}H\}$ CP/MAS NMR spectra of coral septa and thecal wall aragonite: (a) septa and (b) thecal wall of *Desmophyllum dianthus* (DD CHILE TW), (c) septa and (d) thecal wall of *Flabellum* sp. (F MAD TW), (e) live collected (LP CORAL2 75) and (f) fossil (LP COBAS 109) samples of *Lophelia pertusa* thecal wall. (g–h) $^{31}P\{^{1}H\}$ CP/MAS spectra of whole coral samples *Madrepora oculata* (MO CORAL2 75) and *Porites* sp. (PO FR2004), respectively. (i–j) $^{31}P\{^{1}H\}$ CP/MAS spectra of aragonite/phosphate co-precipitates containing (i) 306 μg P/g and (j) 102 μg P/g. All spectra obtained using a spinning rate of 5 kHz, 2 ms CP contact time, and 2 s pulse delay except (h) 10 kHz spinning rate and 120 s pulse delay and (i–j) 2 ms CP contact time, 2 s pulse delay and a spinning rate of 3 kHz. Asterisks mark the location of spinning sidebands.

Table 1
Coral samples studied by ^{31}P NMR, including the location, depth, and dissolved inorganic phosphorus (DIP) concentration of waters in which sample grew at the time of collection. Percentage of the total P contained in apatite (% P_{Ap}) was estimated by NMR (see text); n.d. means none detected. All corals were live at the time of collection unless otherwise indicated. The LA-ICPMS precision (RSD) for the phosphorus concentration is ~ 6% (see methods).

Sample name	Species	Portion	Location	Depth (m)	DIP (μM)	[P] in solid (μg/g)	% P_{Ap}
DD LM99-124	*Desmophyllum dianthus* (fossil)	Septa	Tyrrhenian Sea	377–411	–	119 ± 60	35 ± 5
DD CHILE Coral A	*Desmophyllum dianthus*	Theca	Chilean Fjords	30	1.78 ± 0.36	No data	41 ± 7
DD G16505 S	*Desmophyllum dianthus*	Septa	Western Pacific	406	1.26 ± 0.18	202 ± 55	n.d.
DD G16505 TW	*Desmophyllum dianthus*	Theca	Western Pacific	406	1.26 ± 0.18	17 ± 5	31 ± 5
F MAD S	*Flabellum* sp.	Septa	Madagascar	800–1000	1.99–2.35	87 ± 21	n.d.
F MAD TW	*Flabellum* sp.	Theca	Madagascar	800–1000	1.99–2.35	55 ± 11	34 ± 5
DD CHILE S	*Desmophyllum dianthus*	Septa	Chilean Fjords	30	1.78 ± 0.36	319 ± 79	8 ± 1
DD CHILE TW	*Desmophyllum dianthus*	Theca	Chilean Fjords	30	1.78 ± 0.36	35 ± 7.6	n.d.
LP CORAL2 75	*Lophelia pertusa*	Theca	Ionian Sea	828–818	0.26 ± 0.01	32 ± 12	15 ± 3
LP COBAS 109	*Lophelia pertusa* (fossil)	Theca	Baleares Islands	366	–	106 ± 19	n.d.
MO CORAL2 75	*Madrepora oculata*	Whole coral	Ionian Sea	828–818	0.26 ± 0.01	No data	n.d.
PO FR2004	*Porites* sp.	Whole coral	Fitsroy Reef (Great Barrier Reef)	5	0.12–0.15	36 ± 11	n.d.

3. RESULTS AND DISCUSSION

3.1. ^{31}P SP/MAS and ^{31}P{^{1}H} CP/MAS NMR

3.1.1. ^{31}P SP/MAS NMR of coral samples

We obtained solid-state ^{31}P NMR spectra for both aragonitic azooxanthellate and zooxanthellate coral samples having P contents ranging from 16 to 319 μg/g (Fig. 1 and Table 1), including septa and thecal wall portions as well as whole coral samples. The ^{31}P{^{1}H} CP/MAS and ^{31}P SP/MAS spectra of a *D. dianthus* septum (DD LM99-124) are presented in Fig. 2 and illustrate the typical spectral profile observed for most samples. These spectra can be described by a sum of two Gaussian peaks centered at ^{31}P chemical shifts (δ_P) of 2.7 and 4.0 ppm which have full-widths at half maximum (fwhm) of 1.7 and 6.4 ppm, respectively. Both peaks occur in the chemical shift range typical for orthophosphate species (Turner et al., 1986; Kolowith et al., 2001; Cade-Menun, 2005). Given that the NMR signal arises from the entire sample volume and that the specific surface area of these samples is well below that typically required for observation of signal from surface adsorbed species (ca. 10 $m^2\ g^{-1}$; e.g. Hinedi et al., 1992), the peaks correspond mainly to P contained within the sample interior. One possible host of the P would be a Fe–Mn oxide crust that may not have been removed by the surface abrasion techniques employed, but any P occurring in Fe–Mn-oxides would not be detected under our experimental conditions, owing to extreme peak shifts and broadening of the ^{31}P resonance that would result from magnetic interactions with unpaired electrons (Grey et al., 2010). Therefore, we can rule out P associated with Fe–Mn oxides as the source of the observed ^{31}P NMR signal.

3.1.2. ^{31}P{^{1}H} CP/MAS NMR of coral samples

The two observed peaks exhibit distinct variation in ^{31}P{^{1}H} CP/MAS intensity with contact time (CP kinetics), which allows them to be separated easily according to the acquisition conditions (Fig. 2). The CP kinetics in the simplest cases can be described by a sum of two exponential functions, in which intensity increases at short contact times with a time constant T_{PH} and then decreases at longer times with a time constant $T_{1\rho,H}$ (Kolodziejski and Klinowski, 2002). T_{PH} relates to the spatial proximity of P to H, and $T_{1\rho,H}$ to the relaxation of the ^{1}H nuclei, usually reflecting dynamical processes. The peak at $\delta_P = 2.7$ ppm (Fig. 2a) is dominant at long contact times due to a relaxation time of associated ^{1}H ($T_{1\rho,H} > 10$ ms) that is long compared to that for the peak at $\delta_P = 4.0$ ppm ($T_{1\rho,H} = 1$ ms). We assign the peak at $\delta_P = 2.7$ ppm to crystalline apatite, because its spectral characteristics closely match those reported previously for this mineral, including its chemical shift, narrow width (characteristic of a highly ordered crystalline phase), and long $^{1}H \rightarrow {}^{31}P$ CP time ($T_{PH} = 5$ ms) and $T_{1\rho,H}$ (Rothwell et al., 1980; Belton et al., 1988; Kaflak et al., 2006). The broad peak at $\delta_P = 4.0$ ppm dominates at short contact times (Fig. 2c) because of its much shorter $^{1}H \rightarrow {}^{31}P$ CP time ($T_{PH} = 0.4$ ms). This short T_{PH} value indicates that the P represented by the $\delta_P = 4.0$ ppm peak are spatially close to rigid structural H (separations less than 4 Å). The two peaks fit to the CP/MAS spectra also describe the quantitative SP spectra, indicating that they represent the P distribution in the sample. With few exceptions, the spectra of the other deep-water corals are similar, differing only in the total signal intensity observed and relative proportion of that signal which is attributed to apatite. The chemically cleaned subsamples of *D. dianthus* produce spectra which can be fit with peaks having the same chemical shifts and widths as those observed for the untreated samples. This result indicates that, despite a large reduction in the signal intensity, the P distribution in the cleaned samples is essentially similar to that in the original samples, which had only undergone surface abrasion (Fig. 3).

3.1.3. Identification of additional minor P-species

Two other samples examined contain P chemical environments not found in most of the other deep-water coral

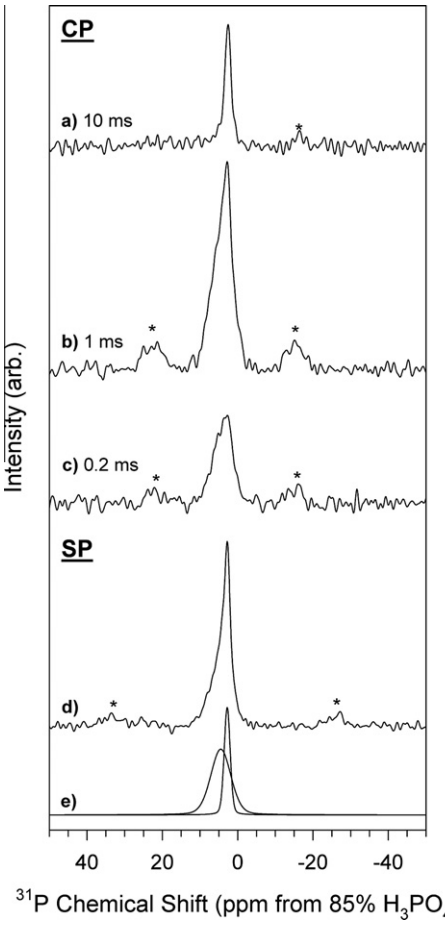

Fig. 2. ^{31}P MAS NMR spectra collected of *Desmophyllum dianthus* coral septa (DD LM99-124) from the Tyrrhenian Sea. (a–c) $^{31}P\{^{1}H\}$ CP/MAS NMR spectra collected at a 3 kHz spinning rate and 2 s pulse delay for 4672 acquisitions using contact times of (a) 10 ms, (b) 1 ms, and (c) 0.2 ms. (d) ^{31}P SP/MAS NMR spectrum obtained with a 5 kHz spinning rate and 120 s pulse delay for 819 acquisitions. (e) Components of the least squares fit to the spectrum shown in (d), vertically offset for clarity.

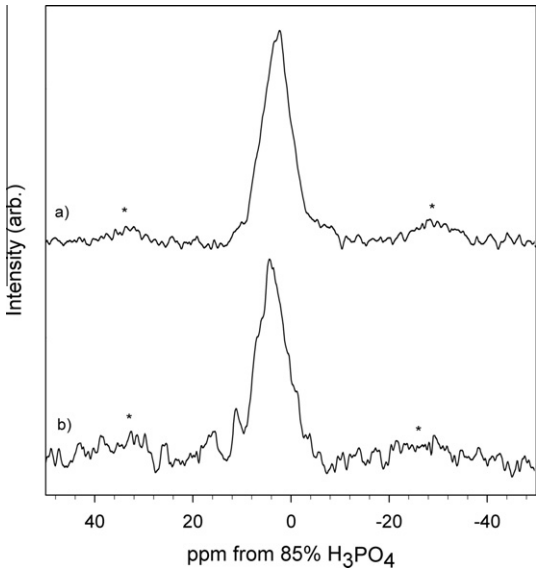

Fig. 3. $^{31}P\{^{1}H\}$ CP/MAS NMR spectra of septa for *Desmophyllum dianthus* sample DD CHILE S collected using 2 s pulse delay and 5 ms CP contact time at a spinning rate of 5 kHz. (a) Spectrum taken from a sample that was only physically cleaned to remove surface contaminants. (b) Spectrum taken from a sample that underwent the chemical treatment outlined by LaVigne et al. (2008). Asterisks mark the location of spinning sidebands.

specimens. Spectra of a *M. oculata* sample (MO CORAL2 75) contain a narrow peak at $\delta_P = -0.6$ ppm (1.1 ppm fwhm), in addition to the broad peak near $\delta_P = 4$ ppm common to all of the coral aragonite examined (Fig. 1g). The small width of the peak at −0.6 ppm suggests that it could arise from a crystalline inorganic phosphate phase (Rothwell et al., 1980; Belton et al., 1988; Mason et al., 2007), but the chemical shift is also consistent with phosphate esters (Cade-Menun, 2005) although such organic-P usually produces broader peaks in solid-state ^{31}P NMR spectra. The origin of this peak was not investigated further, but its presence illustrates that other P-containing materials could be present in coralline aragonite. The *Porites* sp. (PO FR2004) sample we examined yields spectra containing a distinct peak at $\delta_P = 22.5$ ppm (3.0 ppm fwhm), in addition to the broad peak near 4 ppm (Fig. 1h). This 22.5 ppm chemical shift falls outside the range for phosphate, but is diagnostic of phosphonate (Glonek et al., 1970; Kolowith et al., 2001; Cade-Menun, 2005), which contains C–P bonds and indicates the presence of organic P in the sample. The whole skeleton *Madrepora* and *Porites* samples were not physically cleaned, and the sampled areas may include remnant cellular material from either the coral polyp, products of bioerosion, or endosymbionts (the latter refers only to *Porites*). Phosphonates are known to adsorb strongly to calcite surfaces (Sawada et al., 2003; Kan et al., 2005), and could interact similarly with aragonite and become occluded during crystal growth. Since the NMR methods applied here cannot differentiate between organic matter occluded in the aragonite, and that of remnant cellular material, we did not explore these samples further.

3.1.4. ^{31}P NMR of synthetic aragonite/phosphate coprecipitates

A broad peak near $\delta_P = 4$ ppm, similar in terms of chemical shift and width to the broad peak observed for the coral samples, dominates ^{31}P NMR spectra of synthetic aragonite precipitated from solutions containing 1–3 μM DIP (Fig. 1i–j). Several synthetic samples were examined, ranging in P concentration from 100 to 700 μg/g, but their NMR spectra showed no significant differences other than variations in signal intensity consistent with P content. The $^{31}P\{^{1}H\}$ CP kinetics for this broad peak indicate a short $^{1}H \rightarrow {}^{31}P$ CP time ($T_{PH} = 0.3$ ms), similar to that of the broad peak for the coral samples, and a $T_{1\rho,H}$ value that is somewhat longer (4 ms). The ^{31}P CP/MAS spectra of these aragonite/phosphate coprecipitates also contain small, relatively narrow peaks at $\delta_P = 11.4$ and 8.4 ppm (Fig. 1i and j) that are not apparent in the quantitative ^{31}P SP/MAS spectra, suggesting that they arise from

phosphate associated with H in unidentified crystalline phases but represent a small fraction of the P in the samples. A peak for apatite-like orthophosphate was not observed in any of the synthetic samples.

3.2. $^{31}P\{^{1}H\}$ HetCor NMR of coral samples

Since the source of P in the synthetic samples is known, we can assign the resulting NMR signal at $\delta_P = 4$ ppm to inorganic phosphate. Nevertheless, the source of the $\delta_P = 4$ ppm peak in the coral samples cannot be inferred simply by comparison of the ^{31}P data because organic phosphate esters can give NMR peaks in the same ^{31}P chemical shift region (Teleman et al., 1999; Paytan et al., 2003; Cade-Menun, 2005). Distinction between organic and inorganic phosphate can be aided by ^{1}H NMR of the H associated with P, since the ^{1}H chemical shifts of organophosphate aliphatic H, which range from $\delta_H = 2.0$ to 4.0 (Teleman et al., 1999), differ from those typical of HPO_4 groups and structural H_2O which are found, in the 4.0–12.0 ppm range (Yesinowski and Eckert, 1987). We used $^{31}P\{^{1}H\}$ HetCor methods to selectively observe the ^{1}H spectra of only those H located near P, by detecting the ^{1}H from which magnetization is transferred during $^{1}H \rightarrow {}^{31}P$ CP. The ^{31}P-detected ^{1}H spectrum for a sample containing no apatite (DD G16505 S) shows a narrow peak at $\delta_H = 5.5$ ppm that is underlain by a broad peak centered near 7.5 ppm (8.2 ppm fwhm) with a broad spinning sideband pattern (Fig. 4a). Neither peak occurs in the chemical shift range for aliphatic H in organophosphates (Teleman et al., 1999), but are consistent with assignment to molecular water undergoing restricted motion (5.5 ppm) and either rigid structural water or weakly H-bonded hydrogen phosphate (7.5 ppm). The synthetic aragonite/phosphate coprecipitate yielded a ^{31}P-detected ^{1}H spectrum (Fig. 4b) that is similar to that of the coral aragonite, containing a narrow peak at $\delta_H = 6$ ppm and a broader peak centered near 8 ppm with a substantial spinning sideband pattern, but with different relative intensities. Acquisition of each HetCor spectral set required over one week of spectrometer time, making it impractical to collect this data for all the coral samples. Considering that the broad peak near 4 ppm (the main signal in ^{31}P NMR spectra of the coral and synthetic samples) exhibits the same CP kinetics behavior in all samples and that the CP kinetics depends on the nature of H near P, it is reasonable to infer that the hydrogen environments observed in these HetCor spectra represent those associated with P in all samples which yield a similar ^{31}P NMR signal.

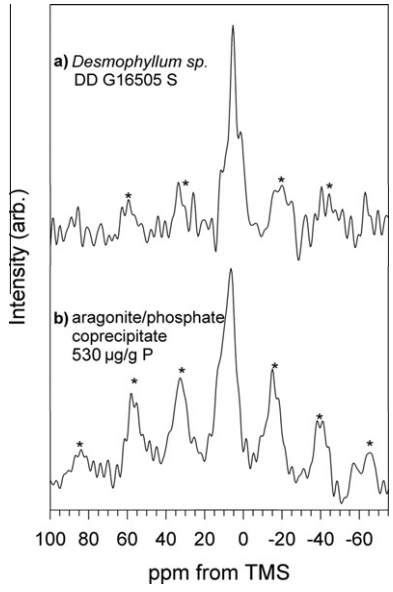

Fig. 4. ^{31}P-detected ^{1}H MAS/NMR spectra obtained from summed projections of 2-d $^{31}P\{^{1}H\}$ CPMG HetCor data for (a) *Desmophyllum dianthus* coral sample DD G16505 S and (b) synthetic aragonite/phosphate coprecipitate (530 µg P/g). Both were collected at 2 ms contact time and 10 kHz spinning rate. Asterisks mark the location of spinning sidebands.

3.3. REDOR NMR

3.3.1. $^{31}P\{^{13}C\}$ REDOR NMR of synthetic aragonite/phosphate coprecipitates

The similarity of both the ^{31}P and (^{31}P-detected) ^{1}H NMR data for the coral aragonite and the synthetic aragonite/phosphate coprecipitate is strong evidence that the nature of the phosphate is the same in both, i.e. orthophosphate. Based only on these NMR data, however, occurrence of phosphate as a substitution defect in the aragonite structure cannot be distinguished from a distinct amorphous Ca-phosphate phase, since the latter yields similar spectra (Rothwell et al., 1980; Kaflak et al., 2006). A test for the presence of phosphate as defects in the aragonite structure can be obtained from a $^{31}P\{^{13}C\}$ REDOR NMR experiment, which depends on atomic-scale spatial proximity between ^{31}P and ^{13}C nuclei (within a few Å; Gullion and Vega, 2005). For this experiment, we used an aragonite/phosphate coprecipitate synthesized with ^{13}C-enriched carbonate because REDOR detects proximity to only the NMR-active ^{13}C isotope, the natural abundance of which (1.1%) is too low to yield a detectable REDOR effect for the very weak ^{31}P signal. The REDOR experiment compares two ^{31}P spectra, a control spectrum (S_0; Fig. 5a and c), containing signal from all P in the sample, and a REDOR spectrum (S; Fig. 5b and d) obtained in a similar manner as for S_0, except that dephasing pulses are applied at the ^{13}C frequency to re-introduce $^{31}P/^{13}C$ dipolar coupling, causing a decrease in signal intensity for P located near ^{13}C. Simulations of the REDOR experiment indicate that no significant decrease in the ^{31}P peak intensity should occur for P located farther than 5 Å from ^{13}C.

The REDOR results at a 6.7 ms dephasing period show a large REDOR fraction $[(S_0 - S)/S_0] = 0.7$ for the broad peak near $\delta_P = 4$ ppm. This value is similar to, but somewhat lower than the maximum REDOR fraction (0.90) that could be expected for a phosphate substituting for a carbonate group (6 C surrounding a central P at a distance of 3.2 Å; Fig. 6) in the aragonite structure, as estimated using the SPINEVOLUTION software (Veshtort and Griffin, 2006). A REDOR fraction smaller than this maximum value would be expected to result from structural disruption

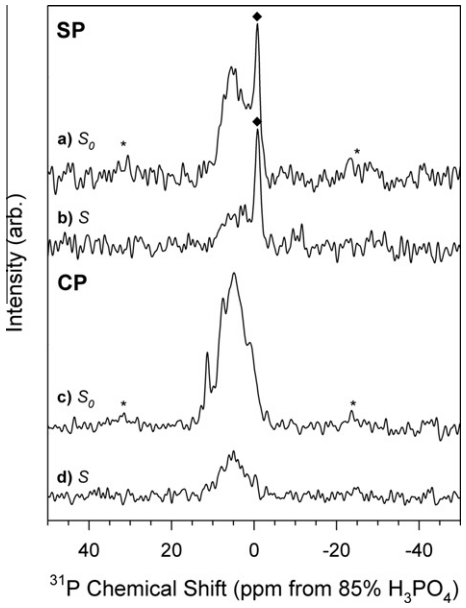

Fig. 5. $^{31}P\{^{13}C\}$ REDOR NMR spectral sets for ^{13}C-enriched aragonite/phosphate coprecipitate collected at a 6 kHz spinning rate and 6.7 ms dephasing period. SP: standard SP/REDOR, CP: CP/REDOR with 2 ms $^{31}P\{^{1}H\}$ CP preparation. (a and d) Echo control spectra (S_0); (b and c) $^{31}P\{^{13}C\}$ REDOR spectra (S). Diamonds denote background signal from rotor and asterisks mark the location of spinning sidebands. S_0, S pairs are plotted at the same absolute intensity.

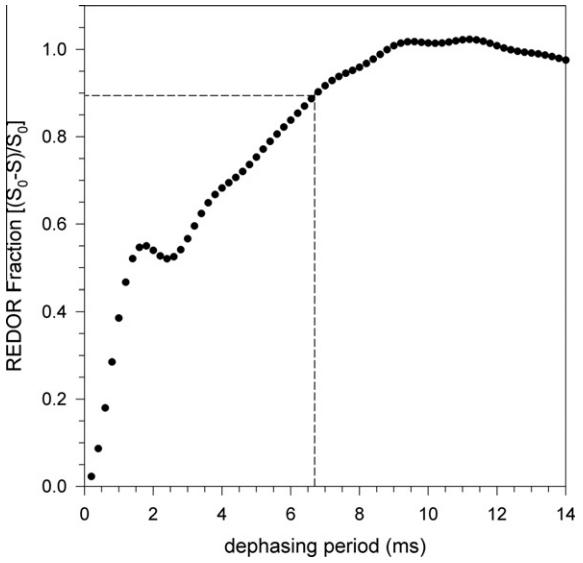

Fig. 6. Simulated $^{31}P\{^{13}C\}$ REDOR dephasing curve for a ^{31}P surrounded by 6 ^{13}C at a distance of 3.2 Å. Dashed line occurs at the dephasing period where experimental data is reported.

around a phosphate defect that would lead to fewer adjacent carbonate groups and/or longer P–C distances. Nevertheless, our simulations indicate that multiple short (<4 Å) P–C distances are required to explain the observed P/C REDOR fraction, which would seem possible only if the phosphate occurs in the structure of the carbonate phase. Similar REDOR results were obtained whether single-pulse (SP) or cross-polarization from ^{1}H (CP) was employed for excitation of ^{31}P (cf. Fig. 5a–d), strongly suggesting that much of the phosphate in aragonite is associated with H, and hence that H-bearing species play a role in accommodating the defect.

3.3.2. $^{1}H\{^{31}P\}$ and $^{19}F\{^{1}H\}$ REDOR NMR of coral samples

To determine the nature of the crystalline apatite inclusions that occur in some coral specimens, $^{1}H\{^{31}P\}$ and $^{19}F\{^{31}P\}$ REDOR NMR experiments were carried out to identify signals from H or F located in close proximity to P. Fluorapatite is a significant sink for phosphate in marine sediments (Kim et al., 1999) whereas biogenic apatite is composed primarily of carbonate-substituted hydroxylapatite (Elliott, 2002). The ^{19}F NMR spectrum of the *Flabellum* sp. theca sample (Fig. 7) is complex and displays multiple peaks. None of these peaks can be assigned to fluorapatite, which would occur at a chemical shift near −102 ppm (Braun and Jana, 1995), nor to any other phase for which ^{19}F NMR data have been reported in the literature. In addition, no $^{19}F\{^{31}P\}$ REDOR effect was observed for any ^{19}F peak, further indicating that no significant fraction of the F is associated with P, and hence that the apatite detected by ^{31}P NMR does not correspond to fluorapatite (Fig. 7). The $^{1}H\{^{31}P\}$ REDOR data (Fig. 8) were obtained for a *D. dianthus* theca wall sample (DD CHILE Coral A). The control spectrum contains peaks at $\delta_H = 4.8$ and 1.5 ppm that do not exhibit decreased intensity in the REDOR spectrum, but which correspond well to signals assigned to water molecules and structural hydroxyl in a previous NMR study of calcium carbonate minerals (Gaffey, 1995). A very small peak occurs near $\delta_H = 0.2$ ppm, near the chemical shift reported for hydroxylapatite

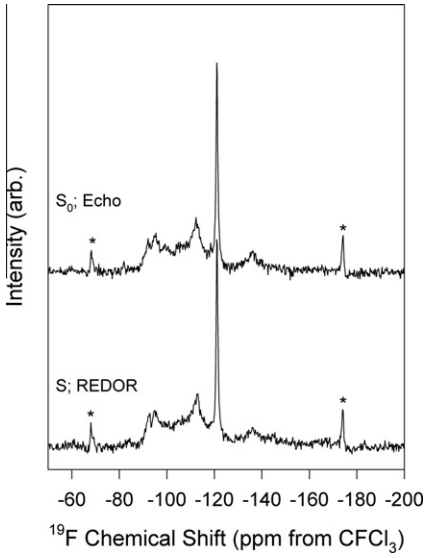

Fig. 7. $^{19}F\{^{31}P\}$ REDOR NMR spectra collected for the *Flabellum* sp. theca sample (F MAD S) collected at a spinning rate of 25 kHz, a 100 s pulse delay, and 1.28 ms dephasing period for 1488 acquisitions. Top: ^{19}F spin-echo control spectrum (S_0). Bottom: $^{19}F\{^{31}P\}$ REDOR spectrum (S). Asterisks mark the location of spinning sidebands.

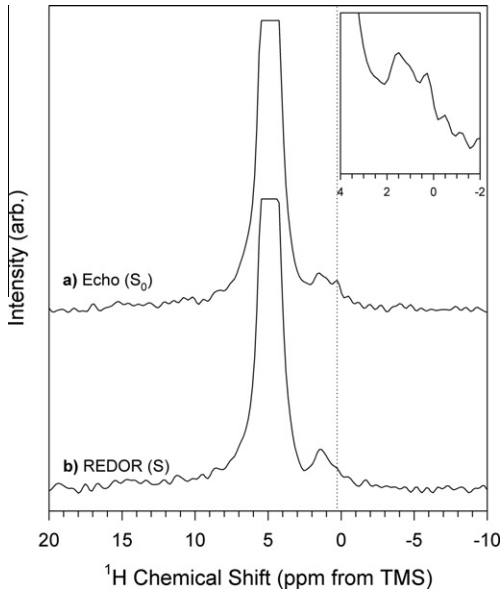

Fig. 8. $^1H\{^{31}P\}$ REDOR NMR spectra for a *Desmophyllum dianthus* (DD CHILE Coral A) sample collected at a spinning rate of 15 kHz, pulse delay of 2 s, and dephasing period of 4.4 ms for 62,928 acquisitions. Spectra are shown at five times vertical exaggeration and truncated. (a) $^1H\{^{31}P\}$ spin-echo control spectrum (S_0). (b) $^1H\{^{31}P\}$ REDOR spectrum (S). Dotted line denotes the chemical shift of hydroxylapatite (0.2 ppm). Inset: expanded view of the spin-echo control spectrum over the range of 4 to −2 ppm.

(Yesinowski and Eckert, 1987), but which is marginally above the noise level. This peak is clearly absent from the $^1H\{^{31}P\}$ REDOR spectrum (cf. Fig. 8a and b), indicating proximity to P and consistent with assignment to hydroxylapatite. These observations support the idea that the narrow peak in $^{31}P\{^1H\}$ CP spectra (Fig. 2a) arises from hydroxylapatite inclusions. Hydroxylapatite can also contain significant amounts of F, but the hydroxyl peak in a mixed OH, F apatite would be expected to occur at a more positive chemical shift of about 1.2–1.4 ppm (Yesinowski and Eckert, 1987).

3.4. Quantification of the ^{31}P NMR signal

3.4.1. Relative hydroxylapatite content

Since acquisition of quantitative ^{31}P NMR spectra is extremely time-consuming, and impractical at P contents less than about 200 μg/g, we developed a relationship between relative intensities in ^{31}P SP/MAS and $^{31}P\{^1H\}$ CP/MAS spectra as a means to estimate the proportion of hydroxylapatite. Ideally, the relative abundances of P corresponding to the peaks at $\delta_P = 2.7$ and 4 ppm would be derived through the careful integration of ^{31}P SP/MAS NMR spectra. However, the low concentration of P in the samples and the long experimental relaxation delays (100's of seconds) needed for quantitative results required almost 4 days of continuous spectrometer time for some samples. Acquisition of a $^{31}P\{^1H\}$ CP/MAS NMR spectrum takes less than half the time to obtain a similar signal to noise ratio, but the results are not quantitative without careful analysis of CP kinetics (Kolodziejski and Klinowski, 2002), which can be time-consuming for the present samples (6–8 spectra are needed, each requiring up to 2 days to acquire). Therefore, we estimated the relative abundance of apatite in the aragonitic coral skeletons from CP/MAS spectra using a correlation between SP/MAS and CP/MAS intensities, similar to that described by Mason et al. (2007). The integrated intensity ratio of the peaks at 4 and 2.7 ppm was determined from a SP spectrum acquired under quantitative conditions for a sample that contained a high fraction of apatite P (*D. dianthus* septa sample: DD LM99-124). The integrated intensities of these peaks are proportional to the number of P in the corresponding environments (e.g., the peak at 2.7 ppm represents $35 \pm 5\%$ of the intensity for sample DD LM99-124, indicating that $35 \pm 5\%$ of the P in this sample occurs in apatite). A correction factor for CP/MAS spectra was then obtained by comparing this SP integrated intensity ratio with that obtained from a CP/MAS spectrum of the same sample (1 ms contact time). This correction factor was applied to the integrated intensity ratios obtained from CP/MAS spectra of the other samples (also taken with 1 ms contact times), yielding estimates for the percentage of the ^{31}P NMR detected P that occurs in apatite (Table 1, last column).

3.4.2. P concentrations in the solid

For several samples, we independently measured P content using solution ICPMS in addition to LA-ICPMS analyses (Table 2). The solution ICPMS data provides an accurate measure of the bulk P content of these samples and any disparity with the LA-ICPMS data was attributed to the fact that the latter only analyzes the outer septal layers and may not accurately reflect the bulk P content which is detected by NMR (Montagna et al., 2009; Anagnostou et al., 2011). We also estimated the bulk P content of several samples from NMR data for comparison to the solution ICPMS results. The $^{31}P\{^1H\}$ CP/MAS NMR intensity of a sample of known bulk P content (synthetic aragonite containing 530 μg/g P as determined from the synthesis method) was compared to that of the unknown, collected under identical acquisition conditions (5 kHz spinning rate, 2 ms contact time, 2.0 s pulse delay) and scaled by mass and number of acquisitions. The synthetic aragonite yielded no detectable signal for apatite in CP/MAS spectra collected under conditions (10 ms contact time) that would favor its observation. We assume that the CP kinetics for the phosphate species are reasonably consistent among samples. Using these methods described above, we estimate 77 ± 12 μg P/g for DD-CHILE-TW, 200 ± 28 μg P/g for LP COBAS 109, and 126 ± 18 μg P/g the DD-CHILE-S samples. The estimated concentration for DD-CHILE-S is in good agreement with that from the solution ICPMS analyses whereas that for LP COBAS 109 is somewhat higher, perhaps owing to the inaccuracy of the NMR method or sample heterogeneity (Table 2). A portion of the sample DD-CHILE-TW that was chemically treated using the method designed to remove surface sorbed metals and metal oxides (DD-CHILE-TW-ct) showed a 54% reduction of P content to 35 ± 5 μg P/g. Nevertheless, its

Table 2
P concentration data for selected coral samples obtained from solution ICPMS and NMR methods. $[P]_{Ap}$ determined from % P_{Ap} values in Table 1. The solution ICPMS precision (RSD) for the P/Ca and P concentration is ~9.5% (see methods). Samples denoted "ct" were chemically treated as described in the text. n.d. means none detected.

Sample	P/Ca (μmol/mol)	$[P]_{ICPMS}$ (μg/g)	$[P]_{NMR}$ (μg/g)	$[P]_{Ap}$ (μg/g)
DD G16505 S	121 ± 11	38 ± 4	No data	n.d.
DD G16505 TW	68 ± 6	22 ± 2	No data	7 ± 1
DD CHILE TW	No data	No data	77 ± 12	n.d.
DD CHILE TW-ct	No data	No data	35 ± 5	n.d.
DD CHILE S	331 ± 31	118 ± 11	126 ± 18	10 ± 1
DD CHILE S-ct	253 ± 24	83 ± 8	No data	No data
LP CORAL2 75	49 ± 5	16 ± 2	No data	2 ± 1
LP COBAS 109	374 ± 36	123 ± 12	200 ± 28	n.d.

^{31}P CP/MAS NMR spectral profile did not differ significantly from that of the untreated material (cf. Fig. 3). Comparison of the solution ICPMS P concentrations with those estimated from CP/MAS NMR spectra indicate that no large fraction of P is undetected by NMR. Although not designed to dissolve the host aragonite, the chemical cleaning procedure utilizes strong acids and oxidizing agents which appears to preferentially remove aragonite around phosphate defects. Despite the loss of material, there does not appear to be a significant difference in the bonding environment of the remaining phosphate.

3.4.3. Absolute hydroxylapatite content

Combining the relative abundance of hydroxylapatite derived from NMR analyses with absolute P-contents from solution ICPMS data for the same sample, the amount of hydroxylapatite can be estimated (Table 2). The result is a wide range of hydroxylapatite contents with no obvious relationship to environmental factors such as depth and DIP. Nor do the concentrations of hydroxylapatite correlate with the absolute P content determined from solution ICPMS. For example, solution ICPMS data indicate that DD G16505 TW contains only 22 μg P/g, but a large percentage, 31%, occurs in hydroxylapatite. Furthermore, there seems to be no relationship between the apatite content and the preservation state of the corals (i.e. alive or fossil; Table 1). This result suggests that the apatite inclusions are not produced solely through diagenetic processes.

3.5. Nature of P in coral aragonite

Previous studies have suggested that the majority of P present in coral skeletons exists as organic P-species (Dodge et al., 1984; Shotyk et al., 1995; LaVigne et al., 2008; Anagnostou et al., 2011). This conclusion is based primarily on the results of various extraction procedures relying on assumptions about the solubility and availability of organic versus inorganic P-species. Since many studies assume that the acid-insoluble fraction contains only organic P, the presence of relatively insoluble Ca-phosphates and possible adsorption of phosphate onto insoluble particles upon release by aragonite dissolution could skew the results of such an assay. The results of the present spectroscopic study clearly show that the principal P-species in most coral aragonite samples closely resembles that produced by simply incorporating dissolved inorganic phosphate in synthetic aragonite.

The chemical cleaning methods employed here were originally designed to remove oxide coatings and metals not incorporated into the aragonite structure. We do observe a substantial decrease in the P concentration of the chemically-treated samples, but we attribute this result to preferential dissolution of phosphate-rich regions, rather than the removal of P associated with Fe–Mn or other metal oxide minerals. The NMR-derived P concentrations for untreated samples are in reasonable agreement with those obtained by solution ICPMS methods for the same samples. If a significant pool of P is associated with Fe–Mn crusts a large discrepancy between these values would be expected due to the inability of the NMR methods employed here to observe P associated with ions having unpaired electrons (Grey et al., 2010).

Montagna et al. (2009) and Anagnostou et al. (2011) have shown that the outer surface of coral septa produce higher LA-ICPMS derived P concentrations than the interior portions. Montagna et al. (2009) attributed these differences to the presence of P-rich species such as hydroxylapatite in the outer septal surface. Since the NMR methods applied here are bulk techniques, we cannot differentiate between P contained in P-rich outer layers and that contained within the less P-rich internal microstructures. Given the results of Montagna et al. (2009), the observed drop in the NMR-derived P concentrations after the application of the chemical cleaning methods could be attributed to the removal of defect and P-rich portions of the coral aragonite which are more susceptible to dissolution.

3.6. Implications for further studies of P proxies in coral

A robust relationship between P/Ca ratio of coral aragonite and DIP, suitable for use as a paleo-nutrient proxy, would seem possible only if P occurs in the aragonite structure as phosphate substitution defects. Simple trace element partitioning models developed for inorganic carbonates have been applied to surface and deep-water coral aragonite (Gaetani and Cohen, 2006; Sinclair and Risk, 2006; Gagnon et al., 2007), with the assumption that the coral polyp precipitates aragonite extracellularly from a calcifying fluid located between the polyp and the previous skeletal aragonite (Cohen and McConnaughey, 2003). This

fluid consists of seawater, which is maintained supersaturated with respect to calcium carbonate through an enzymatic input of Ca^{2+} and removal of $2H^{+}$ (Cohen and McConnaughey, 2003). At least three processes could lead to P incorporation into coral aragonite: encapsulation of surface precipitates, occlusion of organic matter, and co-precipitation of dissolved inorganic phosphate as a substitution defect in the aragonite likely initiated as a surface-adsorption complex. Of these, only in the latter could it be expected that equilibrium is established between surface adsorbed phosphate and dissolved phosphate in the aqueous phase, as required for the application of a linear partition coefficient (Rimstidt et al., 1998; Curti, 1999). Standard methodology used for proxy development such as LA-ICPMS, ion microprobe and X-ray adsorption spectroscopy (XAS) cannot yet provide the molecular-scale spatial relationships between P and carbonate necessary to test whether P occurs in the aragonite structure. The results obtained in the present study suggest that co-precipitation of phosphate at defect sites is the dominant process of P incorporation in deep-water corals, lending support for the use of P/Ca as a proxy. Nevertheless, many of the studied samples also contain significant amounts of apatite that could cause systematic error in proxy relationships, but which is easily detected using the methods described here. Given the limited number of samples examined in the present study, and the results showing the incorporation of organo-P-species in some samples, screening of additional coral samples may also be warranted. Taking into account possible contamination by crystalline inclusions, careful selection of the coral portion to be analyzed (e.g. Montagna et al., 2009; Anagnostou et al., 2011) should make it possible to obtain a more robust P/Ca vs. DIP calibration, useful for paleo-nutrient reconstructions.

ACKNOWLEDGMENTS

We like to thank the associate editor Alfonso Mucci, and three anonymous reviewers whose insightful comments led to significant improvements in this manuscript. This research was supported by the U.S. NSF (EAR-0819838), and instrumentation provided by NSF CHE-03-21001. P. Montagna acknowledges financial support from the Marie Curie International Outgoing Fellowship. Coral collection was funded by CNR grants, ESF Moundforce and EU HERMES and HERMIONE (grant agreement n. 226354) projects; Bruno Briano (Savona, Italy) and Günter Försterra kindly supplied corals from offshore Madagascar and the Chilean fjords, respectively. Ship time on RV Urania was provided by CNR and is gratefully acknowledged. This is ISMAR-Bologna scientific contribution n. 1688. H.M. was supported through a U.S. Dept. of Education sponsored GAANN fellowship (P200A060248).

REFERENCES

Ahlgren J., Brabandere H. D., Reitzel K., Rydin E., Gogoll A. and Waldeback M. (2007) Sediment phosphorus extractants for phosphorus-31 nuclear magnetic resonance analyses: a quantitative evaluation. *J. Environ. Qual.* **36**, 892–898.

Anagnostou E., Sherrell R. M., Adkins J. F. and Gagnon A. C. (2007) Phosphorus, barium and boron in the deep-sea coral *Desmophyllum dianthus*: preliminary calibrations. *Geochim. Cosmochim. Acta* **71**, A22.

Anagnostou E., Sherrell R. M., Gagnon A., LaVigne M., Field M. P. and McDonough W. F. (2011) Seawater nutrient and carbonate ion concentrations recorded as P/Ca, Ba/Ca, and U/Ca in the deep-sea coral *Desmophyllum dianthus*. *Geochim. Cosmochim. Acta* **75**, 2529–2543.

Belton P. S., Harris R. K. and Wilkes P. J. (1988) Solid-state ^{31}P NMR studies of synthetic inorganic calcium phosphates. *J. Phys. Chem. Solids* **49**, 21–27.

Benitez-Nelson C. R. (2000) The biogeochemical cycling of phosphorus in marine systems. *Earth Sci. Rev.* **51**, 109–135.

Braun M. and Jana C. (1995) ^{19}F NMR spectroscopy of fluoridated apatites. *Chem. Phys. Lett.* **245**, 19–22.

Broecker W. S. (1982) Ocean geochemistry during glacial time. *Geochim. Cosmochim. Acta* **46**, 1689–1705.

Cade-Menun B. J. (2005) Characterizing phosphorus in environmental and agricultural samples by ^{31}P nuclear magnetic resonance spectroscopy. *Talanta* **66**, 359–371.

Cheng H., Adkins J., Edwards R. L. and Boyle E. A. (2000) U-Th dating of deep sea corals. *Geochim. Cosmochim. Acta* **64**, 2401–2416.

Cohen A. L. and McConnaughey T. A. (2003) Geochemical perspectives on coral mineralization. *Rev. Min. Geochem.* **54**, 151–187.

Curti E. (1999) Coprecipitation of radionuclides with calcite: estimation of partition coefficients based on a review of laboratory investigations and geochemical data. *Appl. Geochem.* **14**, 433–445.

Dodge R. E., Jickells T. D., Knap A. H., Boyd S. and Bak R. P. M. (1984) Reef-building coral skeletons as chemical pollution (phosphorus) indicators. *Mar. Pollut. Bull.* **15**, 178–187.

Elliott J. C. (2002) Calcium phosphate biominerals. *Rev. Mineral. Geochem.* **48**, 427–453.

Gaetani G. A. and Cohen A. L. (2006) Element partitioning during precipitation of aragonite from seawater: a framework for understanding paleoproxies. *Geochim. Cosmochim. Acta* **70**, 4617–4634.

Gaffey S. J. (1995) H_2O and OH in echinoid calcite: a spectroscopic study. *Am. Mineral.* **80**, 947–959.

Gagnon A. C., Adkins J. F., Fernandez D. P. and Robinson L. F. (2007) Sr/Ca and Mg/Ca vital effects correlated with skeletal architecture in a scleractinian deep-sea coral and the role of Rayleigh fractionation. *Earth Planet. Sci. Lett.* **261**, 280–295.

Glonek T., Henderson T. O., Hilderbrand R. L. and Myers T. C. (1970) Biological phosphonates: determination by phosphorus-31 nuclear magnetic resonance. *Science* **169**, 192–194.

Grey C. P., Kim J., Middlemiss D. S., Chernova N. A., Zhu B. Y. X. and Masquelier C. (2010) Linking local environments and hyperfine shifts: a combined experimental and theoretical ^{31}P and ^{7}Li solid-state NMR study of paramagnetic Fe(III) phosphates. *J. Am. Chem. Soc* **132**, 16825–16840.

Gullion T. and Vega A. J. (2005) Measuring heteronuclear dipolar couplings for $I = 1/2$, $S > 1/2$ spin pairs by REDOR and REAPDOR NMR. *Prog. NMR Spectrosc.* **47**, 123–136.

Hinedi Z. R., Goldberg S., Chang A. C. and Yesinowski J. P. (1992) A ^{31}P and ^{1}H MAS NMR study of phosphate sorption onto calcium carbonate. *J. Colloid Interf. Sci.* **152**, 141–160.

House W. A. and Donaldson L. (1986) Adsorption and coprecipitation of phosphate on calcite. *J. Colloid Interf. Sci.* **112**, 309–324.

LaVigne M., Field M. P., Anagnostou E., Grottoli A. G., Wellington G. M. and Sherrell R. M. (2008) Skeletal P/Ca tracks upwelling in Gulf of Panama coral: evidence for a new seawater phosphate proxy. *Geophys. Res. Lett.* **35**, L05604.

LaVigne M., Matthews K. A., Grottoli A. G., Cobb K. M., Anagnostou E., Cabioch G. and Sherrell R. M. (2010) Coral

skeleton P/Ca proxy for seawater phosphate: multi-colony calibration with a contemporaneous seawater phosphate record. *Geochim. Cosmochim. Acta* **74**, 1282–1293.

Kaflak A., Chmielewski D., Gorecki A., Slorarczyk A. and Kolodziejski W. (2006) Efficiency of $^{1}H \rightarrow {}^{31}P$ cross-polarization in bone apatite and its mineral standards. *Solid State NMR* **29**, 345–348.

Kan A. T., Fu G. M. and Tomson M. B. (2005) Adsorption and precipitation of an aminoalkylphosphonate onto calcite. *J. Colloid Interf. Sci.* **281**, 275–284.

Kim D., Schuffert J. D. and Kastner M. (1999) Francolite authigenesis in California continental slope sediments and its implications for the marine P cycle. *Geochim. Cosmochim. Acta* **63**, 3477–3485.

Kolodziejski W. and Klinowski J. (2002) Kinetics of cross-polarization in solid-state NMR: a guide for chemists. *Chem. Rev.* **102**, 613–628.

Kolowith L. C., Ingall E. D. and Benner R. (2001) Composition and cycling of marine organic phosphorus. *Limnol. Oceanogr.* **46**, 309–320.

Koutsoukos P. G. and Nancollas G. H. (1981) Crystal growth of calcium phosphates: epitaxial considerations. *J. Cryst. Growth* **53**, 10–19.

Mason H. E., Frisia S., Tang Y., Reeder R. J. and Phillips B. L. (2007) Phosphorus speciation in calcite speleothems determined from solid-state NMR spectroscopy. *Earth Planet. Sci. Lett.* **254**, 313–322.

Millero F., Huang F., Zhu X. R., Liu X. W. and Zhang J. Z. (2001) Adsorption and desorption of phosphate on calcite and aragonite in seawater. *Aquat. Geochem.* **7**, 33–56.

Milliman J. D. and Bornhold B. D. (1973) Peak height versus intensity analysis of X-ray diffraction data. *Sedimentology* **20**, 445–448.

Montagna P., McCulloch M., Taviani M., Mazzoli C. and Vendrell B. (2006) Phosphorus in cold-water corals as a proxy for seawater nutrient chemistry. *Science* **312**, 1788–1791.

Montagna P., McCulloch M., Mazzoli C., Silenzi S. and Odorico R. (2007) The non-tropical coral *Cladocora caespitosa* as the new climate archive for the Mediterranean Sea: high-resolution (weekly) trace element systematics. *Quater. Sci. Rev.* **26**, 441–462.

Montagna P., McCulloch M., Taviani M., Trotter J. and Silenzi S. (2009) An improved sampling method for P/Ca as a nutrient proxy. *Geochem. Cosmochim. Acta* **73**, A895.

Morse J. W., Zullig J. J., Bernstein L. D., Millero F. J., Milne P., Mucci A. and Choppin G. R. (1985) Chemistry of calcium carbonate-rich shallow water sediments in the Bahamas. *Am. J. Sci.* **285**, 147–185.

Paytan A., Cade-Menun B. J., McLaughlin K. and Faul K. L. (2003) Selective phosphorus regeneration of sinking marine particles: evidence from ^{31}P-NMR. *Mar. Chem.* **82**, 55–70.

Reeder R. J., Nugent M., Lamble G. M., Tait C. D. and Morris D. E. (2000) Uranyl incorporation into calcite and aragonite: XAFS and luminescence studies. *Environ. Sci. Technol.* **34**, 638–644.

Rimstidt J. D., Balog A. and Webb J. (1998) Distribution of trace elements between carbonate minerals and aqueous solutions. *Geochim. Cosmochim. Acta* **62**, 1851–1863.

Rothwell W. P., Waugh J. S. and Yesinowski J. P. (1980) High-resolution variable-temperature ^{31}P NMR of solid calcium phosphates. *J. Am. Chem. Soc.* **102**, 2637–2643.

Sarmiento J. L., Hughes T. M. C., Stouffer R. J. and Manabe S. (1998) Simulated response of the ocean carbon cycle to anthropogenic climate warming. *Nature* **393**, 245–249.

Sawada K., Abdel-Aal N., Sekino H. and Satoh K. (2003) Adsorption of inorganic phosphates and organic polyphosphonate on calcite. *J. Chem. Soc. Dalton Trans.* **3**, 342–347.

Sinclair D. J. and Risk M. J. (2006) A numerical model of trace-element coprecipitation in a physicochemical calcification system: application to coral biomineralization and trace-element 'vital effects'. *Geochim. Cosmochim. Acta* **70**, 3855–3868.

Shen G. T. and Boyle E. A. (1988) Determination of lead, cadmium, and other trace metals in annually-banded corals. *Chem. Geol.* **67**, 47–62.

Shotyk W., Immenhauserpotthast I. and Vogel H. A. (1995) Determination of nitrate, phosphate and organically bound phosphorus in coral skeletons by ion chromatography. *J. Chromatogr. A* **706**, 209–213.

Teleman A., Richard P., Toivari M. and Penttilla M. (1999) Identification and quantitation of phosphorus metabolites in yeast neutral pH extracts by nuclear magnetic resonance spectroscopy. *Anal. Biochem.* **272**, 71–79.

Turner B. L., Cade-Menun B. J., Condron L. M. and Newman S. (2005) Extraction of soil organic phosphorus. *Talanta* **66**, 294–306.

Turner G. L., Smith K. A., Kirkpatrick R. J. and Oldfield E. (1986) Structure and cation effects on ^{31}P NMR chemical shifts and chemical-shift anisotropies of orthophosphates. *J. Magn. Reson.* **70**, 408–415.

Tyrrell T. (1999) The relative influences of nitrogen and phosphorus on oceanic primary production. *Nature* **400**, 525–531.

Vandecasteele C. and Block C. B. (1997) *Modern methods for trace element determination*. John Wiley and Sons Ltd., West Sussex, England.

Veshtort M. and Griffin R. G. (2006) SPINEVOLUTION: a powerful tool for the simulation of solid and liquid state NMR experiments. *J. Magn. Reson.* **178**, 248–282.

Volk T. and Hoffert M. I. (1985) Ocean carbon pumps: analysis of relative strengths and efficiencies in ocean-driven atmospheric CO_2. In *The Carbon Cycle and Atmospheric CO2: Natural Variations Archean to Present* (eds. E. T. Sundquist and W. S. Broecker). AGU, Washington, DC, pp. 99–110.

Yesinowski J. P. and Eckert H. (1987) Hydrogen environments in calcium phosphates: ^{1}H MAS NMR at high spinning speeds. *J. Am. Chem. Soc.* **109**, 6274–6282.

Zhong S. J. and Mucci A. (1993) Calcite precipitation in seawater using a constant addition technique: a new overall reaction kinetic expression. *Geochim. Cosmochim. Acta* **57**, 1409–1417.

Associate editor: Alfonso Mucci